Formation of secondary organic aerosols from the reaction of γ-terpinene with ozone: yields and morphology

Layal Fayad, Cécile Coeur, Nicolas Houzel, Karine Deboudt, Xavier Sécordel, Hichem Bouzidi, Gaël Mouret

Formation of secondary organic aerosols from the reaction of γ-terpinene with ozone: yields and morphology

Layal Fayad, Cécile Coeur*, Nicolas Houzel, Karine Deboudt, Xavier Sécordel, Hichem Bouzidi, Gaël Mouret

Laboratoire de Physico-Chimie de l'Atmosphère, Université du Littoral Côte d'Opale, 189A Avenue Maurice Schumann, Dunkerque, France

*Corresponding author. Tel.: +33 328 23 76 42

Email address: coeur@univ-littoral.fr (C. Coeur).

Abstract

Atmospheric secondary organic aerosols (SOAs), formed from condensable oxidation products of anthropogenic and biogenic volatile organic compounds (VOCs), are important constituents of the atmosphere accounting for a significant fraction of ambient tropospheric aerosol. In this study, the formation of SOAs from the gas-phase ozonolysis of γ-terpinene (1-isopropyl-4-methyl-1,4-cyclohexadiene), a monoterperne emitted by many different trees (elm, cypress, water hickory, maple trees…) has been studied in an indoor atmospheric simulation chamber (CHARME), at 294 ± 2 K, atmospheric pressure, under dry conditions (relative humidity, RH < 2%) and in absence of seed particles. The concentration of γ-terpinene was measured by a proton transfer reaction - time of flight - mass spectrometer (PTR-ToF-MS), that of ozone by an UV photometric analyzer and the aerosol mass concentration was monitored using a scanning

mobility particle sizer (SMPS). Scanning electronic microscopy (SEM) observations were performed to characterize the physical state and morphology of the formed SOAs. They show the formation of spherical aerosols in a viscous state.

The overall organic aerosol yield (Y) was determined as the ratio of the suspended aerosol mass concentration corrected for wall losses (M_o) to the total reacted γ-terpinene concentration, assuming a particle density of 1 g cm^{-3}. The aerosol formation yield increases as the initial γ-terpinene concentration increases. The presence of an OH radical scavenger (cyclohexane) leads to a decrease in the SOA yields (they varied from 0.11 to 0.54 and from 0.16 to 0.49, without and with, an OH radical scavenger, respectively). Y is a strong function of M_o and the organic aerosol formation can be expressed by a one-product gas/particle partitioning absorption model.

Keywords: simulation chamber, γ-terpinene ozonolysis, secondary organic aerosols

1. Introduction

Biogenic sources dominate the global emission budget of volatile organic compounds into the atmosphere, with monoterpenes accounting for 11 % of non-methane hydrocarbons emitted (Guenther et al., 1995; Sindelarova et al., 2014). Monoterpenes play an important role in atmospheric chemistry, they impact its oxidative capacity, the tropospheric ozone budget and produce secondary organic aerosols (SOAs). In the atmosphere, aerosols influence climate (Huang et al., 2007; Tomasi and Lupi, 2016), reduce visibility (Yu et al., 2016) and affect human health (Chung and Seinfeld, 2002; Kim et al., 2015; Hallquist et al., 2009; Pye et al., 2010). The gas-phase reaction of ozone with monoterpenes has been largely studied and it is now recognized that it is an important source of SOAs (Bateman et al., 2009; Berndt et al., 2003; Griffin et al.,

1999; Herrmann et al., 2010; Lee et al., 2006; Ma et al., 2007; Pathak et al., 2007; Saathoff et al., 2009; Shilling et al., 2008, 2009; Walser et al., 2008).

The products formed, both in the gas- and particle- phases, from the ozonolysis of monoterpenes, display significant variability due to the structural differences of the different compounds. For example, monoterpenes with one C=C double bond like α-pinene ($k_{\alpha\text{-pinene + O3}} = 9.6\times10^{-17}$ cm^3 molecule^{-1} s^{-1} ; IUPAC, current recommendation) or β-pinene ($k_{\beta\text{-pinene + O3}} = 1.9\times10^{-17}$ cm^3 molecule^{-1} s^{-1}; IUPAC, current recommendation), are less reactive toward ozone than those with 2 C=C double bonds like limonene ($k_{\text{limonene + O3}} = 2.2\times10^{-16}$ cm^3 molecule^{-1} s^{-1}; IUPAC, current recommendation), α-phellandrene ($k_{\alpha\text{-phellandrene + O3}} = 2.9\times10^{-15}$ cm^3 molecule^{-1} s^{-1}; IUPAC, current recommentation) or γ-terpinene ($k_{\gamma\text{-terpinene + O3}} = (2.10 \pm 0.11)\times10^{-16}$ cm^3 molecule^{-1} s^{-1}; Fayad et al., 2021). Biogenic emissions are complex and only a few compounds have been studied, so this is important to account for the variability of monoterpenes to develop accurate atmospheric chemistry models. Nevertheless, in the literature most of the studies have predominantly focused on the most abundant emitted monoterpenes (e.g. α-pinene, β-pinene, limonene (Lee et al., 2006 ; Saathoff et al., 2009; Mackenzie-Rae et al., 2017).

γ-Terpinene (1-isopropyl-4-methyl-1,4-cyclohexadiene; molecular structure provided in Fig. 1) is a monoterpene emitted by many different trees (elm, cypress, waterhickory, maple trees…). It contributes to less than 10% of total monoterpene emissions by mass and relatively little data on its atmospheric reactivity are available in the literature. This work contributes to study the differences in chemistry between monoterpene isomers. In the atmosphere, the volume ratios of γ-terpinene are about a few pptv (Bouvier-Brown et al., 2009). With two endocyclic C=C double bonds, this compound is highly reactive toward OH radical ($k_{OH} = 1.7 \times 10^{-10}$ cm^3 molecule^{-1} s^{-1}

(Atkinson et al., 1986)), NO_3 radical (k_{NO3} = 2.9 x 10^{-11} cm^3 $molecule^{-1}$ s^{-1} (Atkinson et al., 1985)) and ozone (k_{O3} = (1.63 - 2.17) × 10^{-16} cm^3 $molecule^{-1}$ s^{-1} cm^3 $molecule^{-1}$ s^{-1} (Grimsrud et al., 1975; Atkinson et al., 1990 and Fayad et al., 2021)).

The aim of the present work was to study the potential of SOA formation from the ozone reaction with γ-terpinene. The experiments were performed in the chamber CHARME, in the dark, at (294 ± 2) K, atmospheric pressure and low relative humidity (RH < 2 %), with and without an scavenger (cyclohexane) and in absence of seed particles. The overall aerosol yields were determined and the data analyzed according to the absorptive gas-particle partitioning model developed by Pankow (1994 a,b) and Odum et al. (1996). The SOA formation yields have been compared with those resulting from a recent study on the ozone reaction with γ-terpinene (Xu et al., 2020). The morphology of the aerosols was investigated using scanning electronic microscopy (SEM) observations. The atmospheric implications of the reaction of γ-terpinene with ozone are also discussed.

This article dedicated to the study of secondary organic aerosols completes a previous one in which kinetic and gaseous products formed from the γ-terpinene reaction with ozone were investigated (Fayad et al., 2021).

2. Material and methods

This study was carried out in the new chamber CHARME (CHamber for the study of the Atmospheric Reactivity and the Metrology of the Environment), designed in the LPCA (Laboratoire de Physico-Chimie de l'Atmosphere) laboratory in Dunkerque (France). The chamber is described in detail in (Fayad, 2019), briefly it consists of a 9.2 m^3 evacuable cylinder (length ≈ 4 m; internal diameter ≈ 1.7 m ; surface to volume ratio ≈ 3.5 m^{-1}) made in stainless

steel (304 L) and electropolished. Four stainless steel fans (diameter 50 cm) located at the bottom of the chamber provide located at the bottom assure a rapid homogenization of gases and particles. The relative humidity and temperature within the chamber were monitored by a combined probe (Vaisala HUMICAP, HMT330). The CHARME chamber was pumped down to 0.4 mbar with a vacuum pump (Cobra NC0100-0300B) and was then filled till the atmospheric pressure with purified and dried air using a generator (Parker Zander KA-MT 1-8). After the chamber cleaning, satisfactory background particle number concentrations below 5 particles cm^{-3} were measured.

γ-Terpinene was first injected into the chamber using a glass impinger and its concentrations were monitored versus the time (every 10 seconds) using a proton transfer reaction time of flight mass spectrometer (PTR-ToF-MS 1000, IONICON Analytik, Innsbruck, Austria). The detailed principle of the PTR-ToF-MS is described in Blake et al., (2009). Briefly, this instrument allows to quantify chemical compounds having a proton affinity higher than that of water. Briefly, VOCs are ionized via a proton transfer reaction and are then identified from their mass to charge ratios (m/z). The air from the chamber was sampled through an inlet PEEK capillary line of 100 cm heated at 333 K to reduce the loss of the VOCs during their sampling and then ionized in the drift tube (E = 600 $V.cm^{-1}$; E/N=136 Td) operating at 2.2 mbar and 333 K. γ-Terpinene concentrations were recorded from the signal of the ion at m/z 137.2, corresponding to its parent $[M-H]^+$ ion. In the PTR-ToF-MS, the γ-terpinene fragmentation was observed and this compound was detected at m/z 81.0 (≈ 65%) and m/z 137.2 (≈ 35%). However, as the main peak interfered with some oxidation products formed during the ozonolysis reaction, it was not selected to monitor the concentrations of γ-terpinene.

Ozone was injected into the chamber with a corona discharge generator (Air Tree Ozone Technology C-L010-DTI) that converts pure O_2 into O_3 and the ozone concentrations were measured using an UV photometric analyzer (Thermo Scientific 49i). The ozone wall loss ($k_{wall(O3)} = (2\text{-}3) \times 10^{-5}\ s^{-1}$), which follows a first order law, was determined in experiments were ozone was solely introduced in the chamber.

The SOA formation was followed versus the time with a Scanning Mobility Particle Sizer (SMPS TSI, CPC 3775 / DMA 3081) using a 2 min scan time and a 16 s delay between samples, providing a size distribution between 15 nm and 661 nm. The aerosol mass concentration M_O was calculated assuming an aerosol density of 1.0.

Background SOA formation could occur from the ozone reaction with off-gasing of compounds from the chamber walls and/or with impurities of the purified air. This particle formation was investigated from the dark reaction of purified air with ozone and led to an aerosol mass concentrations of 0.1 µg m^{-3}, which was negligible compared to the SOA mass concentrations determined from the reaction of O_3 with γ-terpinene (in the range 10 - 907 µg m^{-3}). The SOA concentrations in the chamber were corrected for particle wall loss. The aerosol wall loss, which is described by a first order law with a dependence on the aerosol size, was measured during ≈1 h in the end of each experiment once γ-terpinene was totally consumed and the ozone concentration reach a plateau, indicating that chemistry isn't still occurring.

The plots of $\ln[M_O]_0/\ln[M_O]_t$ versus the time, where M_O is the aerosol mass concentration (in µg m^{-3}) and the subscripts 0 and t correspond to the aerosol concentrations once the aerosol production has stopped and at a time t, respectively. The aerosol wall loss rates estimated in this

137 work varied from 0.01 to 0.03 h^{-1}. These values are in the same than those obtained in other
138 simulation chambers (Henry et al., 2008; Hurley et al., 2001; Lauraguais et al., 2012, 2014).
139 Preliminary experiments were performed to verify the linearity of the PTR-MS with respect to
140 the γ-terpinene concentrations. The wall losses of this compound as well as those of ozone were
141 also investigated in the dark from the decay of their concentrations when they were solely
142 injected in the chamber. The wall losses followed a first order law and led to values around $9 \times$
143 10^{-6} s^{-1} and 2×10^{-5} s^{-1} for γ-terpinene and ozone, respectively.
144 It is known that the ozonolysis of alkenes produces OH radicals which are formed from the
145 rearrangement of Criegee biradicals (Atkinson et al., 1992; Aschmann et al., 2002; Kroll et al.,
146 2002), So, to evaluate the effect of the OH radicals in the SOA formation, a series of experiments
147 were performed using cyclohexane as an OH scavenger. The concentrations of cyclohexane were
148 calculated in order to scavenge more than 95% of the hydroxyl radicals formed (i.e.
149 $k_{(cyclohexane+OH)} \times [cyclohexane] / k_{(\gamma\text{-terpinene}+OH)} \times [\gamma\text{-terpinene}] \geq 10$).
150 The morphology of the SOAs formed from the γ-terpinene reaction with ozone was observed by
151 scanning electronic microscopy (SEM). A Dekati 3-stages cascade impactor (with cut-off
152 diameters at 10, 1 µm and 30 nm) was connected to the chamber to sample aerosols on TEM
153 grids. Each collection plate was covered by a polycarbonate membrane on which two grid types
154 were fixed: Lacey carbon film or carbon formvar film on 300 Mesh Copper TEM Grids (Agar
155 Scientific). At the end of the experiment, aerosols were collected at 8 L min^{-1} for 5 minutes.
156 Then, the SOAs were observed by cryo-electron microscopy using a field effect gun-SEM
157 coupled with a transmitted electron detector (JEOL 7100F FEG-TSEM), equipped with three
158 Energy Dispersive X-ray (EDS, Bruker X Flash 6/30) spectrometers and a Quorum PP3010P
159 cryostage. For that, the sample is vitrified by an ultra-rapid freezing by plunging them in liquid

nitrogen, and then transfer on the cryo-stage of the microscope with a liquid nitrogen cooled cryo-TEM holder. This preparation allows to determine the size and morphology of atmospheric particles in the vacuum of the microscope without modification of these parameters in comparison with the ambient temperature (Veghte et al., 2014), by limiting their damage due to the electron beam. Data and pictures were acquired at 15 kV, 300 pA and 10 mm for the working distance and at a temperature of -100° C.

The compounds used in this study, their manufacturer and stated purity were: γ-terpinene (ACROS; 97%), cyclohexane (CHEM-LAB; ≥ 99.5%) and pure dioxygen (PRAXAIR; 99.9999%)

3. Results and Discussion

3.1. SOA formation yields

A total of 13 experiments were performed in CHARME at 294 ± 2 K, atmospheric pressure, under dry conditions (relative humidity, RH < 2%) and in absence of seed particles, to determine the SOA formation yields formed from the ozonolysis reaction of γ-terpinene in the presence (6 experiments) and absence (7 experiments) of an OH radical scavenger (cyclohexane). In Table 1 are displayed: the γ-terpinene initial mixing ratios ($[\gamma\text{-terp}]_0$; from 16 ppbv to 328 ppbv); the ozone initial mixing ratios ($[O_3]_0$; from 60 ppbv to 625 ppbv); the γ-terpinene reacted concentrations (Δ[γ-terp]); the organic aerosol mass concentrations corrected for wall losses (M_0) and the aerosol overall yields (Y). The experiments were conducted until the mass concentrations of the SOAs formed reach a plateau (i.e for a reaction time of about 15-30 min). The SOA yields were experimentally determined as the ratio of the organic aerosols formed (M_O in μg m^{-3}) to the reacted γ-terpinene concentration (Δ[γ-terp] in μg m^{-3}) at the end of each experiment:

183 $$Y = \frac{M_O}{\Delta[\gamma\text{-terp}]} \quad \text{(Eq. 1)}$$

184

185 The organic aerosol mass concentration was calculated from the total organic aerosol volume,
186 assuming a density of 1 g cm^{-3} in consistence with the studies of Wirtz and Martin-Reviejo
187 (2003) and Wang et al. (2011) for the α-pinene ozonolysis. An uncertainty of about 30% is
188 estimated on the SOA yield values, taking into consideration the systematic and statistical errors
189 on M_O and Δ[γ-terp].
190 The experimental data displayed in Table 1 show that the aerosol formation is strongly affected
191 by the initial monoterpene concentration: an increase of the γ-terpinene initial concentrations
192 leads to the formation of higher SOA mass concentrations as well as larger aerosol yields. This
193 observation is in agreement with the reactivity, as increasing the initial concentrations of the
194 organic precursor produce higher amounts of condensable products. Moreover, as the organic
195 aerosol mass directly affects the gas/particle partitioning by acting as the medium into which
196 oxidation products can be absorbed, higher SOA masses lead to higher SOA yields.
197 Typical time profiles of γ-terpinene, ozone and SOA mass concentrations are presented in Fig. 2
198 together with time-dependent aerosol size distributions (experiment #3; initial conditions: γ-
199 terpinene (117 ppbv) and O_3 (424 ppbv). The first minutes of the reaction, showed a fast increase
200 in the particle number concentration followed by a gradual decrease throughout the experiment.
201 The particle mean diameters started at ≈ 50 nm and the aerosol growth led to final mean
202 diameters at ≈ 120 nm after 60 min. The particle mass concentration increases during the course
203 of the experiment and reaches a plateau after about 15 min of reaction, which is consistent with a
204 slower reaction rate due to the reduction of the precursor concentrations.

This behavior is explained by the occurrence of initial nucleation step that forms a burst of particles which then undergo coagulation. Nucleation is driven by supersaturation of condensable products such as highly oxygenated organic molecules (HOMs) that have extremely low volatility (Xavier et al., 2019). The formation of extremely low volatility organic compounds (ELVOCs) was recorded within the first minute after the injection of ozone in monoterpenes ozonolysis systems (Jokinen et al., 2015; Xu et al., 2020).

Under atmospheric conditions, stabilised Criegee intermediates (SCI) react with water molecules and their decomposition becomes negligible. In contrast, under dry conditions, SCI decomposition occurs, which leads to smaller molecules and reduces the formation of secondary organic aerosols. So, we could expect than in the atmosphere, the γ-terpinene reaction with ozone forms higher SOA yields than those measured in the simulation chamber under a relative humidity of 2 %. However, Li et al. (2019) have studied the ozonolysis of α-pinene, limonene, and Δ3-carene under a range of RH (from ~3 % to ~92 %) in a temperature-controlled flow tube to generate secondary organic aerosol (SOAs). A major finding from this work is that neither the detected highly oxidized molecules (HOMs) nor their abundance changed significantly with RH. Nevertheless, as RH increased, the total SOA number concentrations decreased by a factor of 2–3, while SOA mass concentrations remained relatively constant. In addition, Zhu et al. (2017) have shown the non-dependence characteristics between relative humidity and SOA formed from isoprene.

Fig. 3 displays the variation of the SOA mass concentration (M_O) versus the γ-terpinene reacted concentration (Δ[γ-terp]) obtained at the end of each experiment (each data point represents a separate experiment). Strong linear correlations for data obtained both in absence ($R^2 = 0.99$) and in presence ($R^2 = 0.98$) and an OH radical scavenger (cyclohexane) is observed, with slopes of 0.54 and 0.49 respectively. These latter values correspond to the maximum SOA yields measured for the ozonolysis reaction of γ-terpinene both without ($Y_{max} = 0.54$) and with cyclohexane,

229 respectively (see table 1), so they represent the upper limit of the SOA yields for this reaction.
230 Table 1 shows that the SOA yields formed from the ozonolysis of γ-terpinene without an OH
231 radical scavenger are higher than those obtained with the scavenger; they range from 0.11 to 0.54
232 and from 0.16 to 0.49, respectively. Cyclohexane has been shown to reduce SOA yields in
233 different ozonolysis reactions, with cyclohexene (Keywood et al., 2004), α-phellandrene
234 (Mackenzie-Rae et al., 2017) and limonene (Saathoff et al., 2009; Gong et al., 2018). The
235 addition of cyclohexane as OH scavenger suppresses the reaction between γ-terpinene and
236 hydroxyl radicals and forms RO_2 radicals from the cyclohexane oxidation by OH. These C_6-RO_2
237 (RO_2 with 6 carbon atoms) can react with other C_6-RO_2 and also with C_{10}-RO_2 formed from the
238 γ-terpinene ozonolysis. These accretion reactions lead to the formation of products having
239 shorter carbonaceous chains and a higher volatility than those formed between C_{10}-RO_2. So, the
240 SOA formation yields obtained without cyclohexane are higher than those measured with this
241 OH scavenger. The observation of lower SOA masses in the present work when OH scavenger
242 was added indicates that the γ-terpinene hydroperoxides (i.e. the vinyl ROOH generated from the
243 isomerization of Criegee intermediates; Fayad et al., 2021) may be more volatile than the
244 products resulting from RO_2 + RO_2 reactions. In addition, particle-phase reactions implying OH
245 radicals may also be invoked. For example, Iinuma et al. (2005) showed that OH radicals play an
246 important role in the particle-phase reactions leading to oligomeric species. Therefore,
247 scavenging OH radicals precludes the formation of such low volatile species and leads to a
248 decrease of the SOA mass and yield.
249 The organic aerosol yields measured in this study can be described by a widely-used semi-
250 empirical model based on absorptive gas-particle partitioning of semi-volatile products (Odum et

al., 1996; Pankow, 1994 a,b). In this model, the SOA yield (Y) of a particular hydrocarbon is expressed by the following equation:

$$Y = \sum_i M_0 \frac{\alpha_i K_{om,i}}{1 + K_{om,i} M_O} \quad \text{(Eq. 2)}$$

α_i is the mass-based gas-phase stoichiometric fraction of the semi volatile product *i*, $K_{om,i}$ the gas-particle partitioning equilibrium constant and M_0 the total aerosol mass concentration (which corresponds to the SOA mass concentration formed as no seeds were used in this study). The yield curve (i. e. the plot of the SOA yields versus of the organic aerosol mass concentrations formed (M_O) in presence and absence of cyclohexane) is shown in Fig. 4. Eq. 2 can be fitted to the γ-terpinene data to determine the values for α_i and $K_{om,i}$. The experimental values are well described by a one-product model and lead to the following values: with cyclohexane ($\alpha = 0.54 \pm 0.05$ and $K = (6.1 \pm 2.0) \times 10^{-3}$ m^3 μg^{-1}; $R^2 = 0.96$;) and without cylcohexane ($\alpha = 0.56 \pm 0.02$ and $K = (13.0 \pm 3.0) \times 10^{-3}$ m^3 μg^{-1} ; $R^2 = 0.98$). The use of two or more products in the model did not improve the quality of the fits and also exhibited high uncertainties on K values. The one-product model suggests that the oxidation products that contribute to most SOA formation are all falling into a similar volatility range. In this case, α_i and $K_{om,i}$ do not have any intrinsic physical meaning but rather represents average values.

The SOA yields measured in this work are compared in Fig. 5 to the experimental data obtained in similar studies investigating the ozonolysis of different monoterpenes in the presence of cyclohexane: α-pinene (Saathoff et al., 2009), limonene (Gong et al., 2018; Saathoff et al., 2009), α-phellandrene (Mackenzie-Rae et al., 2017), terpinolene (Keywood et al., 2004) and γ-terpinene (Xu et al., 2020). For comparison and to take into account that different SOA types could

273 actually have different density, the mass-dependent yield data of the different monoterpenes
274 reported in literature were recalculated using an SOA density of (1.5 ± 3) g cm^{-3}.
275 As shown in Fig. 5, the SOA yields obtained in this study are in very good agreement with those
276 of Xu et al. (2020) who studied the formation of organic aerosols from the gas phase reaction of
277 ozone with γ-terpinene. The comparison of the yield curves obtained from the ozonolysis of
278 different monoterpenes shows that the SOA formation potential is dependent on the molecular
279 structures of the isomers (Griffin et al., 1999). Limonene and α-phellandrene contribute to higher
280 SOA yields than γ-terpinene and terpinolene, indicating that the position of the two C=C double
281 bonds plays an important role in the production of SOAs. For α-phellandrene, the formation of
282 semi-volatile organic compounds was likely driven by the presence of the two conjugated
283 endocyclic C=C double bonds, with functionalisation rather than fragmentation dominating the
284 chemical mechanism of its reaction with ozone (Lee et al., 2006; Mackenzie-Rae et al., 2017).
285 Limonene, with one endocyclic and one exocyclic C=C double bond exhibits similar SOA yields
286 to α-phellandrene. For limonene, the reaction of the endocyclic C=C double bond results in the
287 formation of unsaturated multifunctional ring-opening products (dicarbonyls, diacids, carbonyled
288 acids…) having a $C=CH_2$ double bond which can then be oxidized into a C=O bond (Gong et al.,
289 2018). This mechanism leads to the formation of C9 compounds with a low volatility which can
290 easily partition in the particulate phase.
291 Terpinolene, with an endo- and an exo- cyclic C=C double bonds, displays the lowest SOA
292 formation yields. In this compound, the exocyclic double bond with its great degree of
293 substitution, is oxidized at first followed by the ozonolysis of the endocyclic double bond which
294 leads to the dissociation of the carbon skeleton and the formation of products with high vapor
295 pressure resulting in reduced SOA yields (Keywood et al., 2004).

296 γ-terpinene displays two endocyclic C=C double bonds. The ozone reaction with one endocyclic
297 C=C double bond leads to unsaturated multifunctional ring-opening products (first generation
298 products), which then react with ozone to form second (or further) generation products. Fayad et
299 al. (2021) have shown that the main oxidation products observed in the gas-phase are C1-C6
300 compounds (formic acid, glyoxal, acetone, 3-oxobutanal, 4-methyl-3-oxopentanal, acetic acid,
301 acetaldehyde, formaldehyde, 3-oxopropanoic acid). This result is in agreement with lower SOA
302 formation yields observed from the ozonolysis of γ-terpinene than from that of limonene.
303
304 α-Pinene displays SOA yields which are intermediate between those determined from the
305 ozonolysis of limonene and α-phellandrene and those from γ-terpinene and terpinolene. This
306 observation is in accordance with the choice of α-pinene as the proxy monoterpene to represent
307 all monoterpenes in some models (particularly global climate models).
308
309 **SOA morphology and physical state**
310 The formation, properties and transformation of organic particles are strongly affected by their
311 physical state (Abramson et al., 2013). Recent modeling studies have pointed out that aerosol
312 morphology, mixing state and viscosity highly impact gas-particle partitioning as well as
313 multiphase and heterogeneous chemistry (Marcolli and Krieger, 2020). Consequently, it is
314 required to understand the different parameters that govern the physical state and morphology of
315 atmospheric particles.
316 Fig. 6 displays the scanning electron microscope (SEM) images of particles collected at the end
317 of experiments γ-terpinene#4 and γ-terpinene#10 performed without and with an OH radical
318 scavenger (cyclohexane), respectively. The aerosols follow the shape of the Lacey film revealing

319 that the SOAs formed from the ozonolysis reaction of γ-terpinene are viscous whether
320 cyclohexane is present or not. These observations agree with numerous investigations
321 (Mikhailov et al., 2009; Virtanen et al., 2010) which provided evidence that atmospheric organic
322 aerosols exist as semi-solid viscous particles. As an example, the viscosity at 30°C of SOAs
323 formed in simulation chamber from the ozonolysis of monoterpenes ranges from 6.2×10^{5} to
324 8.0×10^{8} Pa, so this indicates that these aerosols are in a semi-solid state (Champion et al.,
325 2019).The studies of Virtanen et al. (2010), Shiraiwa et al. (2011) and Kuwata and Martin (2012)
326 also demonstrated that the SOAs produced from ozonolysis of α-pinene could be present in
327 highly viscous semi-solid state at low relative humidity. The viscosity of organic aerosols can
328 impact the diffusion of chemical species through particles so the aerosol oxidation rate, with
329 implications for predicting their chemical composition and hygroscopicity (Marshall et al.,
330 2016).
331 The SEM image of SOAs collected on a carbon formvar film (see Fig. 6) shows the formation of
332 rounded shape particles typical to spherical aerosols. These results are in agreement with
333 Virtanen et al., (2010) who observed (using SEM imagery) that biogenic organic aerosols
334 sampled in the boreal forest are also nearly spherical. Among atmospheric particles, spherical
335 ones have the lowest specific surface areas, so the lowest exchange surface between gaseous and
336 particle phases. So, this influences heterogeneous and multiphase chemistry and thermodynamic
337 equilibrium between the gas and condensed phases (Krieger et al., 2012). As an example, the
338 oxidation of atmospheric spherical particle by gaseous oxidant is limited compared to that of
339 rough and/or elongated particles with higher specific surface areas.

340 The formation of solid particles probably results from the condensation of high molecular mass
341 compounds including oxygenated compounds and functional groups that favor the creation of
342 solid phases.
343
344 **Conclusion**
345 The formation of secondary organic aerosols from the ozonolysis reaction of γ-terpinene has
346 been investigated in the simulation chamber CHARME, at 294 ± 2 K, atmospheric pressure,
347 under dry conditions (relative humidity, RH < 2%) and in absence of seed particles. Two sets of
348 experiments were carried out, in the presence and absence of an OH radical scavenger
349 (cyclohexane). The SOA formation yields were dependent on the initial precursor concentration,
350 with higher values obtained when the initial γ-terpinene concentration raised. In addition, a
351 decrease of the aerosol yields was observed in experiments performed with cyclohexane. This
352 result is in agreement with a previous work which shows that the presence of OH radical scavengers
353 reduce the yields of organic aerosols formed from different monoterpene ozonolysis (Docherty et
354 al., 2005). A one product gas-particle partitioning absorption model has been successfully applied
355 to describe the formation of organic aerosols. The atmospheric aerosol concentrations are ≈ 5 µg
356 m^{-3} in many environments and can reach ≈ 50 µg m^{-3} or more in highly polluted environments.
357 Considering these particle loadings, the extrapolation of the data shown in Fig. 4, leads to SOA
358 formation yields around 2 % and 22 %, respectively. Even though, no experimental data points
359 were obtained for Mo = 5 µg m^{-3}, these values agree with those obtained in experiments γ-
360 terpinene#1 (Mo = 10 µg m^{-3} and Y = 11 %) and experiments γ-terpinene#2 (Mo = 69 µg m^{-3} and
361 Y = 27 %) and suggest that the contribution of the ozonolysis reaction of γ-terpinene to SOA
362 production is relatively minor in most of the areas, but can be significant in polluted ones.

Indeed, although, BVOCs are much less likely to be emitted in urban areas compared to forested areas, it has been observed that these compounds can negatively impact the air quality in cities, like in Los Angeles (Nussbaumer and Cohen, 2021).

The morphology and physical state of the formed SOAs were observed using scanning electronic microscopy imagery. The organic aerosols formed from the ozonolysis reaction of γ-terpinene display a spherical shape and are in a viscous state.

Finally, the results presented in this study contribute to substantially improve our knowledge on the differences in chemistry between monoterpene isomers. The comparison between the SOA formation yields obtained from the ozonolysis of different monoterpene shows that α-pinene displays SOA yields which are intermediate between those of other isomers and agree with the choice of α-pinene as the proxy monoterpene to represent all monoterpenes in some models (particularly global climate models).

Acknowledgment

This work was supported by the CaPPA project (Chemical and Physical Properties of the Atmosphere) funded by the French National Research Agency (ANR-11-LABX-0005-01) and the CLIMIBIO program supported by the Hauts-de-France Regional Council, the French Ministry of Higher Education and Research and the European Regional Development Fund. The PhD grant of Layal Fayad was funded by ULCO (Université du Littoral - Côte d'Opale) and PMCO (Pôle Métropolitain Côte d'Opale).

References

Abramson, E., Imre, D., Beránek, J., Wilson, J., Zelenyuk, A., 2013. Experimental determination of chemical diffusion within secondary organic aerosol particles. Phys. Chem. Chem. Phys. 15, 2983. https://doi.org/10.1039/c2cp44013j

Aschmann, S.M., Arey, J., Atkinson, R., 2002. OH radical formation from the gas-phase reactions of O3 with a series of terpenes. Atmos. Environ. 36, 4347–4355. https://doi.org/10.1016/S1352-2310(02)00355-2

Atkinson, R., Aschmann, S.M., Pitts, J.N., 1986. Rate constants for the gas-phase reactions of the OH radical with a series of monoterpenes at 294 ± 1 K: Gas-phase reactions of OH radicals. Int. J. Chem. Kinet. 18, 287–299. https://doi.org/10.1002/kin.550180303

Atkinson, Roger., Aschmann, S.M., Winer, A.M., Pitts, J.N., 1985. Kinetics and atmospheric implications of the gas-phase reactions of nitrate radicals with a series of monoterpenes and related organics at 294 ± 2 K. Environ. Sci. Technol. 19, 159–163. https://doi.org/10.1021/es00132a009

Atkinson, R., Hasegawa, D., Aschmann, S.M., 1990. Rate constants for the gas-phase reactions of O_3 with a series of monoterpenes and related compounds at 296K±2 K. Int. J. Chem. Kinet. 22, 871–887.

Atkinson, R., Aschmann, S.M., Arey, J., Shorees, B., 1992. Formation of OH radicals in the gas phase reactions of O_3 with a series of terpenes. J. Geophys. Res. 97, 6065. https://doi.org/10.1029/92JD00062

Blake, R.S., Monks, P.S., Ellis, A.M., 2009. Proton-Transfer Reaction Mass Spectrometry. Chem. Rev. 109, 861-896. https://doi.org/10.1021/cr800364q

Bouvier-Brown, N.C., Goldstein, A.H., Gilman, J.B., Kuster, W.C., de Gouw, J.A., 2009. In-situ ambient quantification of monoterpenes, sesquiterpenes, and related oxygenated compounds during BEARPEX 2007: implications for gas- and particle-phase chemistry. Atmos. Chem. Phys. 14, 5505-5518.

Champion, W.M., Rothfuss, N.E., Petters, M.D., Grieshop, A.P., 2019. Volatility and Viscosity Are Correlated in Terpene Secondary Organic Aerosol Formed in a Flow Reactor. Environ. Sci. Technol. Lett. 6, 513–519. https://doi.org/10.1021/acs.estlett.9b00412

Docherty, K.S., Wu, W., Lim Y. B., Ziemann, P.J., 2005. Contributions of Organic Peroxides to Secondary Aerosol Formed from Reactions of Monoterpenes with O_3. Environ. Sci. Technol., 39, 4049-4059.

Chung, S. H. and Seinfeld, J. H., 2002. Global distribution and climate forcing of carbonaceous aerosols. J. Geophys. Res., 107, 4407- https://doi.org/10.1029/2001JD001397.

Fayad, L., 2019. Caractérisation de la nouvelle chambre de simulation atmosphérique CHARME et étude de la réaction d'ozonolyse d'un COV biogénique, le γ-terpinène (These de doctorat). Université du Littoral-Côte-d'Opale.

Fayad L., Coeur C., Fagniez T., Secordel X., Houzel N., Mouret G. 2021. Kinetic and mechanistic study of the gas-phase reaction of ozone with γ-terpinene. Atmos. Environ. 246, 118073. DOI: https://doi.org/10.1016/j.atmosenv.2020.118073.

Gong, Y., Chen, Z., Li, H., 2018. The oxidation regime and SOA composition in limonene ozonolysis: roles of different double bonds, radicals, and water. Atmospheric Chem. Phys. 18, 15105–15123. https://doi.org/10.5194/acp-18-15105-2018

Griffin, R.J., Cocker, D.R., Flagan, R.C., Seinfeld, J.H., 1999. Organic aerosol formation from the oxidation of biogenic hydrocarbons. J. Geophys. Res. Atmospheres 104, 3555–3567. https://doi.org/10.1029/1998JD100049

Grimsrud E.P, Westberg H.H, Rasmussen R.A, 1975. Atmospheric reactivity of monoterpene hydrocarbons, NOx photooxidation and ozonolysis. Int. J. Chem. Kinet., 7(1): 183-195.

433 Guenther, A., Hewitt, C.N., Erickson, D., Fall, R., Geron, C., Graedel, T., Harley, P.,
434 Klinger, L., Lerdau, M., Mckay, W.A., Pierce, T., Scholes, B., Steinbrecher, R., Tallamraju, R.,
435 Taylor, J., Zimmerman, P., 1995. A global model of natural volatile organic compound
436 emissions. J. Geophys. Res. 100, 8873. https://doi.org/10.1029/94JD02950
437 Hallquist, M., Wenger, J.C., Baltensperger, U., Rudich, Y., Simpson, D., Claeys, M.,
438 Dommen, J., Donahue, N.M., George, C., Goldstein, A.H., Hamilton, J.F., Herrmann, H.,
439 Hoffmann, T., Iinuma, Y., Jang, M., Jenkin, M.E., Jimenez, J.L., Kiendler-Scharr, A., Maenhaut,
440 W., McFiggans, G., Mentel, T.F., Monod, A., Prevot, A.S.H., Seinfeld, J.H., Surratt, J.D.,
441 Szmigielski, R., Wildt, J., 2009. The formation, properties and impact of secondary organic
442 aerosol: current and emerging issues. Atmos. Chem. Phys. 82.
443 Henry, F., Coeur-Tourneur, C., Ledoux, F., Tomas, A., Menu, D., 2008. Secondary organic
444 aerosol formation from the gas phase reaction of hydroxyl radicals with m-, o- and p-cresol.
445 Atmos. Environ. 42, 3035–3045.
446 Huang, Y., Chameides, W.L., Dickinson, R.E., 2007. Direct and indirect effects of
447 anthropogenic aerosols on regional precipitation over east Asia. J. Geophys. Res. Atmospheres
448 112. https://doi.org/10.1029/2006JD007114
449 Hurley, M.D., Sokolov, O., Wallington, T.J., Takekawa, H., Karasawa, M., Klotz, B.,
450 Barnes, I., Becker, K.H., 2001. Organic aerosol formation during the atmospheric degradation of
451 toluene. Environ. Sci. Technol. 35, 1358–1366.
452 Iinuma, Y., Böge, O., Miao, Y., Sierau, B., Gnauk, T., Herrmann, H., 2005. Laboratory
453 studies on secondary organic aerosol formation from terpenes. Faraday Discussions, 130(15), 1-
454 16.

Jokinen, T., Berndt, T., Makkonen, R., Kerminen, V.-M., Junninen, H., Paasonen, P., Stratmann, F., Herrmann, H., Guenther, A.B., Worsnop, D.R., Kulmala, M., Ehn, M., Sipilä, M., 2015. Production of extremely low volatile organic compounds from biogenic emissions: Measured yields and atmospheric implications. Proc. Natl. Acad. Sci. 112, 7123–7128. https://doi.org/10.1073/pnas.1423977112

Khalil, M.A.K., Rasmussen, R.A., 1992. Forest Hydrocarbon Emissions: Relationships Between Fluxes and Ambient Concentrations. J. Air Waste Manag. Assoc. 42, 810-813. https://doi.org/10.1080/10473289.1992.10467033

Keywood, M.D., Kroll, J.H., Varutbangkul, V., Bahreini, R., Flagan, R.C., Seinfeld, J.H., 2004. Secondary Organic Aerosol Formation from Cyclohexene Ozonolysis: Effect of OH Scavenger and the Role of Radical Chemistry. Environ. Sci. Technol. 38, 3343–3350. https://doi.org/10.1021/es049725j

Kim, K.-H., Kabir, E., Kabir, S., 2015. A review on the human health impact of airborne particulate matter. Environ. Int. 74, 136–143. https://doi.org/10.1016/j.envint.2014.10.005

Krieger, U.K., Marcolli, C., Reid, J.P., 2012. Exploring the complexity of aerosol particle properties and processes using single particle techniques. Chem. Soc. Rev. 41, 6631–6662. https://doi.org/10.1039/C2CS35082C

Kroll, J.H., Donahue, N.M., Cee, V.J., Demerjian, K.L., Anderson, J.G., 2002. Gas-phase ozonolysis of alkenes: formation of OH from anti carbonyl oxides. J. Am. Chem. Soc. 124, 8518–8519. https://doi.org/10.1021/ja0266060

Kuwata, M., Martin, S.T., 2012. Phase of atmospheric secondary organic material affects its reactivity. Proc. Natl. Acad. Sci. 109, 17354–17359. https://doi.org/10.1073/pnas.1209071109

Lauraguais, A., Coeur-Tourneur, C., Cassez, A., Seydi, A., 2012. Rate constant and secondary

organic aerosol yields for the gas-phase reaction of hydroxyl radicals with syringol (2,6 dimethoxyphenol). Atmos. Environ. 55, 43-48.

Lauraguais, A., Coeur-Tourneur, C., Cassez, A., Deboudt, K., Fourmentin, M., Choël, M., 2014. Atmospheric reactivity of hydroxyl radicals with guaiacol (2-methoxyphenol), a biomass burning emitted compound: Secondary organic aerosol formation and gas-phase oxidation products. Atmos. Environ. 86, 155–163. https://doi.org/10.1016/j.atmosenv.2013.11.074

Lee, A., Goldstein, A.H., Keywood, M.D., Gao, S., Varutbangkul, V., Bahreini, R., Ng, N.L., Flagan, R.C., Seinfeld, J.H., 2006. Gas-phase products and secondary aerosol yields from the ozonolysis of ten different terpenes. J. Geophys. Res. 111. https://doi.org/10.1029/2005JD006437

Li, X., Chee, S., Hao, J., Abbatt, J. P. D., Jiang, J., and Smith, J. N.: Relative humidity effect on the formation of highly oxidized molecules and new particles during monoterpene oxidation, Atmos. Chem. Phys., 19, 1555–1570, https://doi.org/10.5194/acp-19-1555-2019, 2019.

Liu, S., Jiang, X., Tsona, N.T., Lv, C., Du, L., 2019. Effects of NOx, SO_2 and RH on the SOA formation from cyclohexene photooxidation. Chemosphere 216, 794–804. https://doi.org/10.1016/j.chemosphere.2018.10.180

Mackenzie-Rae, F.A., Liu, T., Deng, W., Saunders, S.M., Fang, Z., Zhang, Y., Wang, X., 2017. Ozonolysis of α-phellandrene – Part 1: Gas- and particle-phase characterisation. Atmospheric Chem. Phys. 17, 6583–6609. https://doi.org/10.5194/acp-17-6583-2017

Marcolli, C., Krieger, U.K., 2020. Relevance of Particle Morphology for Atmospheric Aerosol Processing. Trends Chem. 2, 1–3. https://doi.org/10.1016/j.trechm.2019.11.008

Marshall, F.H., Miles, R.E.H., Song, Y.-C., Ohm, P.B., Power, R.M., Reid, J.P., Dutcher, C.S., 2016. Diffusion and reactivity in ultraviscous aerosol and the correlation with particle viscosity. Chem. Sci. 7, 1298–1308. https://doi.org/10.1039/C5SC03223G

503 Mikhailov, E., Vlasenko, S., Martin, S.T., Koop, T., Pöschl, U., 2009. Amorphous and
504 crystalline aerosol particles interacting with water vapor: conceptual framework and
505 experimental evidence for restructuring, phase transitions and kinetic limitations. Atmospheric
506 Chem. Phys. 9, 9491–9522. https://doi.org/10.5194/acp-9-9491-2009
507 C. M. Nussbaumer, R. C. Cohen. Impact of OA on the Temperature Dependence of PM 2.5
508 in the Los Angeles Basin Environ. Sci. Technol. 2021, 55, 6, 3549–3558.
509 https://doi.org/10.1021/acs.est.0c07144
510 Odum, J.R., Hoffmann, T., Bowman, F., Collins, D., Flagan, R.C., Seinfeld, J.H., 1996.
511 Gas/Particle Partitioning and Secondary Organic Aerosol Yields 6.
512 Pankow, J.F., 1994a. An absorption model of gas/particles partitioning of organic
513 compounds in the atmosphere. Atmos. Environ. 28, 185–188.
514 Pankow, J.F., 1994b. An absorption model of the gas/aerosol partitioning involved in the
515 formation of secondary organic aerosol. Atmos. Environ. 28, 189–193.
516 Pye, H. O. T., Chan, A. W. H., Barkley, M. P., Seinfeld, J. H. 2010. Global modeling of
517 organic aerosol: the importance of reactive nitrogen (NOx and NO_3), Atmos. Chem. Phys., 10,
518 11261-11276. https://doi.org/10.5194/acp-10-11261-2010.
519 Saathoff, H., Naumann, K.-H., Möhler, O., Jonsson, \AAM, Hallquist, M., Kiendler-Scharr,
520 A., Mentel, T.F., Tillmann, R., Schurath, U., 2009. Temperature dependence of yields of
521 secondary organic aerosols from the ozonolysis of α-pinene and limonene. Atmospheric Chem.
522 Phys. 9, 1551-1577.
523 Shilling, J.E., Chen, Q., King, S.M., Rosenoern, T., Kroll, J.H., Worsnop, D.R., McKinney,
524 K.A., Martin, S.T., 2008. Particle mass yield in secondary organic aerosol formed by the dark

525 ozonolysis of α-pinene. Atmospheric Chem. Phys. 8, 2073–2088. https://doi.org/10.5194/acp-8-
526 2073-2008

527 Shiraiwa, M., Ammann, M., Koop, T., Poschl, U., 2011. Gas uptake and chemical aging of
528 semisolid organic aerosol particles. Proc. Natl. Acad. Sci. 108, 11003–11008.
529 https://doi.org/10.1073/pnas.1103045108.

530 Sindelarova, K., Granier, C., Bouarar, I., Guenther, A., Tilmes, S., Stavrakou, T., Müller, J.-
531 F., Kuhn, U., Stefani, P., and Knorr, W., 2014. Global data set of biogenic VOC emissions
532 calculated by the MEGAN model over the last 30 years, Atmos. Chem. Phys., 14, 9317–9341,
533 https://doi.org/10.5194/acp-14-9317-2014.

534 Tomasi, C., Lupi, A., 2016. Primary and Secondary Sources of Atmospheric Aerosol, in:
535 Tomasi, C., Fuzzi, S., Kokhanovsky, A. (Eds.), Atmospheric Aerosols. Wiley-VCH Verlag
536 GmbH & Co. KGaA, Weinheim, Germany, pp. 1–86.
537 https://doi.org/10.1002/9783527336449.ch1

538 Virtanen, A., Joutsensaari, J., Koop, T., Kannosto, J., Yli-Pirilä, P., Leskinen, J., Mäkelä,
539 J.M., Holopainen, J.K., Pöschl, U., Kulmala, M., Worsnop, D.R., Laaksonen, A., 2010. An
540 amorphous solid state of biogenic secondary organic aerosol particles. Nature 467, 824–827.
541 https://doi.org/10.1038/nature09455

542 Veghte, D.P., Bittner, D.R., Freedman, M.A., 2014. Cryo-Transmission Electron Microscopy
543 Imaging of the Morphology of Submicrometer Aerosol Containing Organic Acids and
544 Ammonium Sulfate. Anal. Chem. 86, 2436–2442. https://doi.org/10.1021/ac403279f

545 Wang, J., Doussin, J.F., Perrier, S., Perraudin, E., Katrib, Y., Pangui, E., Picquet-Varrault,
546 B., 2011. Design of a new multi-phase experimental simulation chamber for atmospheric

547 photosmog, aerosol and cloud chemistry research. Atmospheric Meas. Tech. 4, 2465–2494.
548 https://doi.org/10.5194/amt-4-2465-2011
549 Wirtz, Martin-Reviejo, 2003. Density of secondary organic aerosols. J. Aerosol Sci. 34,
550 S223–S224.
551 Xavier, C., Rusanen, A., Zhou, P., Dean, C., Pichelstorfer, L., Roldin, P., Boy, M., 2019.
552 Aerosol mass yields of selected biogenic volatile organic compounds – a theoretical study with
553 nearly explicit gas-phase chemistry. Atmospheric Chem. Phys. 19, 13741–13758.
554 https://doi.org/10.5194/acp-19-13741-2019
555 Xu, L., Tsona, N.T., You, B., Zhang, Y., Wang, S., Yang, Z., Xue, L., Du, L., 2020. NOx
556 enhances secondary organic aerosol formation from nighttime γ-terpinene ozonolysis. Atmos.
557 Environ. 225, 117375. https://doi.org/10.1016/j.atmosenv.2020.117375
558 Yu, X., Ma, J., An, J., Yuan, L., Zhu, B., Liu, D., Wang, J., Yang, Y., Cui, H., 2016. Impacts
559 of meteorological condition and aerosol chemical compositions on visibility impairment in
560 Nanjing, China. J. Clean. Prod. 131, 112–120. https://doi.org/10.1016/j.jclepro.2016.05.067
561 Zhu, J., Penner, J.E., Yu, F., Sillman, S., Andreae, M.O., Coe, H., 2019. Decrease in
562 radiative forcing by organic aerosol nucleation, climate, and land use change. Nat. Commun. 10
563 (1), 1e7, 423.
564

Fig. 1. γ-terpinene molecular structure.

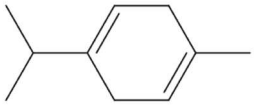

Fig. 2. Typical concentration-time profiles obtained for γ-terpinene (PTR-ToF-MS), O_3 (photometric analyzer) and SOAs (SMPS; measured and corrected for wall losses). Experiment γ-terpinene#3 (without cyclohexane; initial mixing ratios: γ-terpinene (117 ppbv) and O_3 (424 ppbv)).

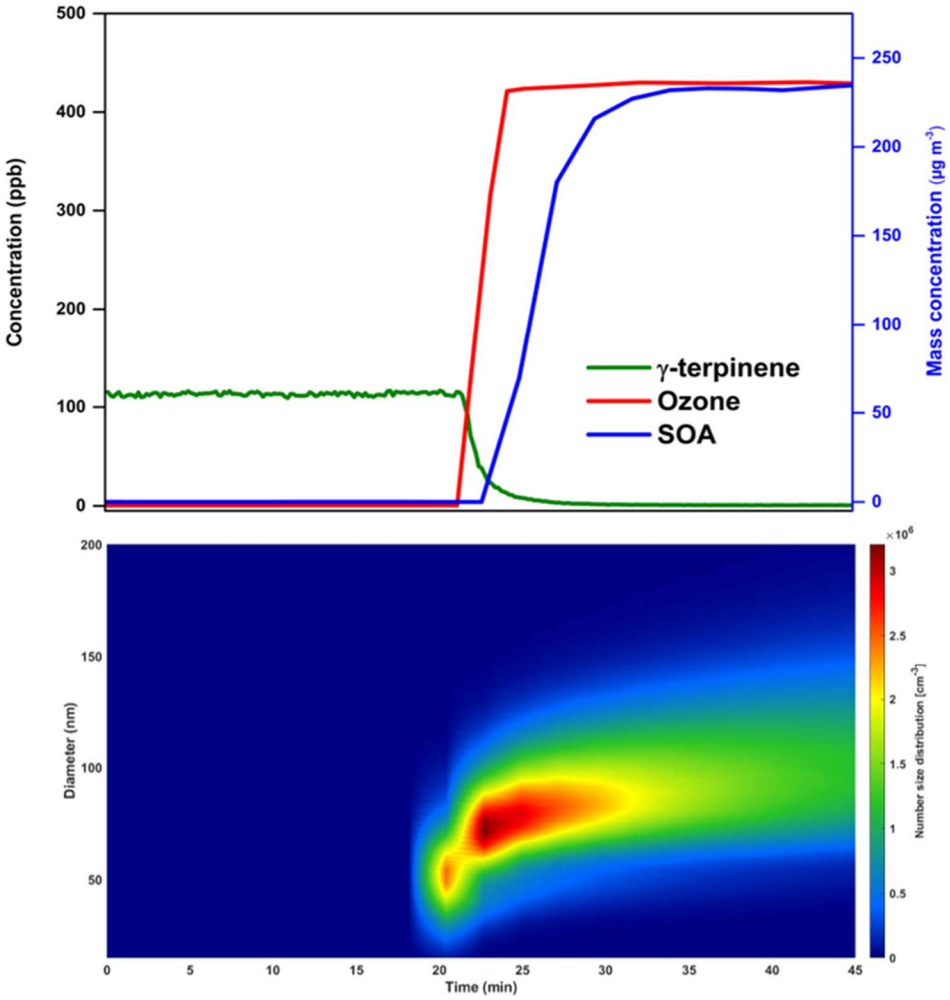

Fig. 3. Plot of the SOA mass concentration versus the reacted γ-terpinene concentration. Each data point represents a separate experiment in presence (open circle) or absence (filled circle) of an OH radical scavenger (cyclohexane). The error bars represent average uncertainties of 20 % on both the measurement of SOA mass and γ-terpinene reacted concentrations.

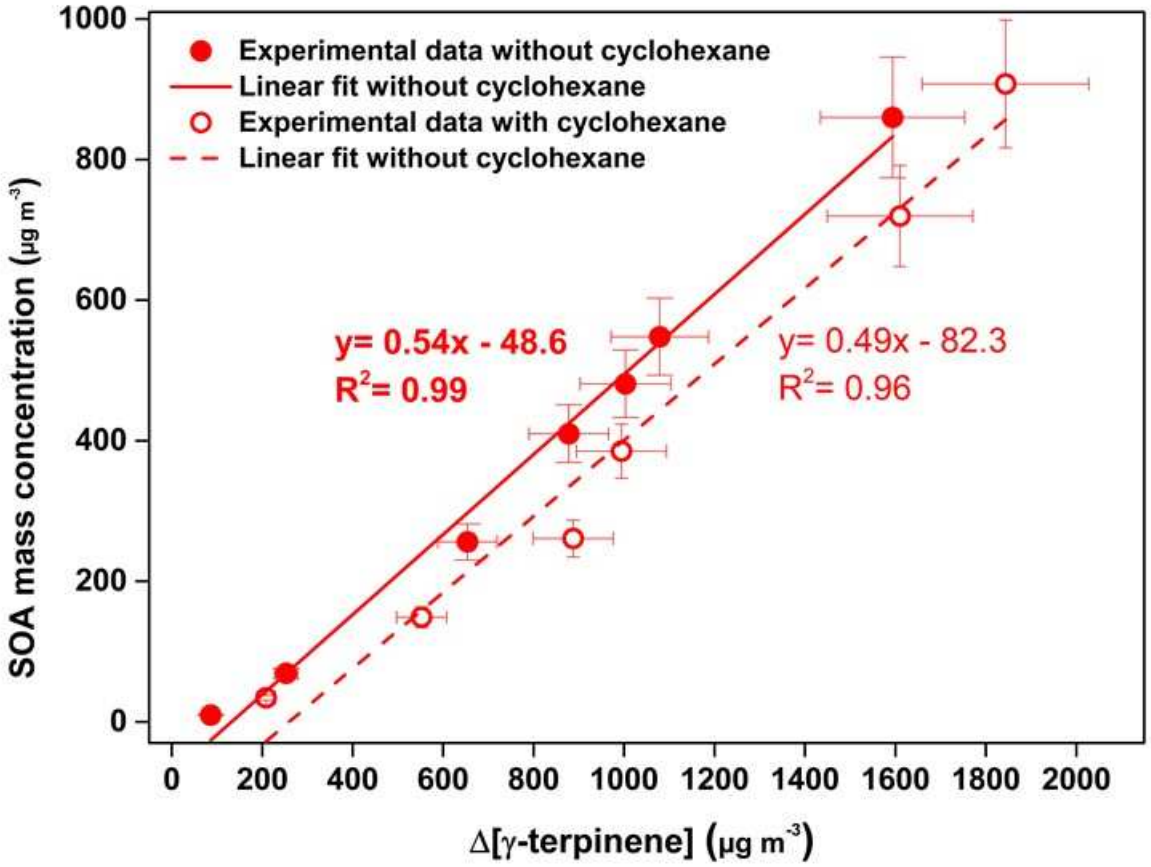

Fig. 4. SOA yields as a function of the organic aerosol mass concentrations formed (M_O) for the ozonlysis reaction of γ-terpinene in presence (open circles) and absence (filled circles) of an OH radical scavenger (cyclohexane). The dotted and straight lines represent the best fits to the data considering a one-product model (with and without cyclohexane, respectively). The fitting parameters are $\alpha = 0.54 \pm 0.05$ and $K_{om} = (6.6 \pm 2.1) \times 10^{-3}$ m^3 μg^{-1} (with cyclohexane; $R^2 = 0.79$) and $\alpha = 0.56 \pm 0.02$ and $K_{om} = (13.0 \pm 3.0) \times 10^{-3}$ m^3 μg^{-1} (without cyclohexane; $R^2 = 0.69$). The error bars represent average uncertainties of 20 % and 40 %, on the measurement of the SOA mass concentrations and yields, respectively.

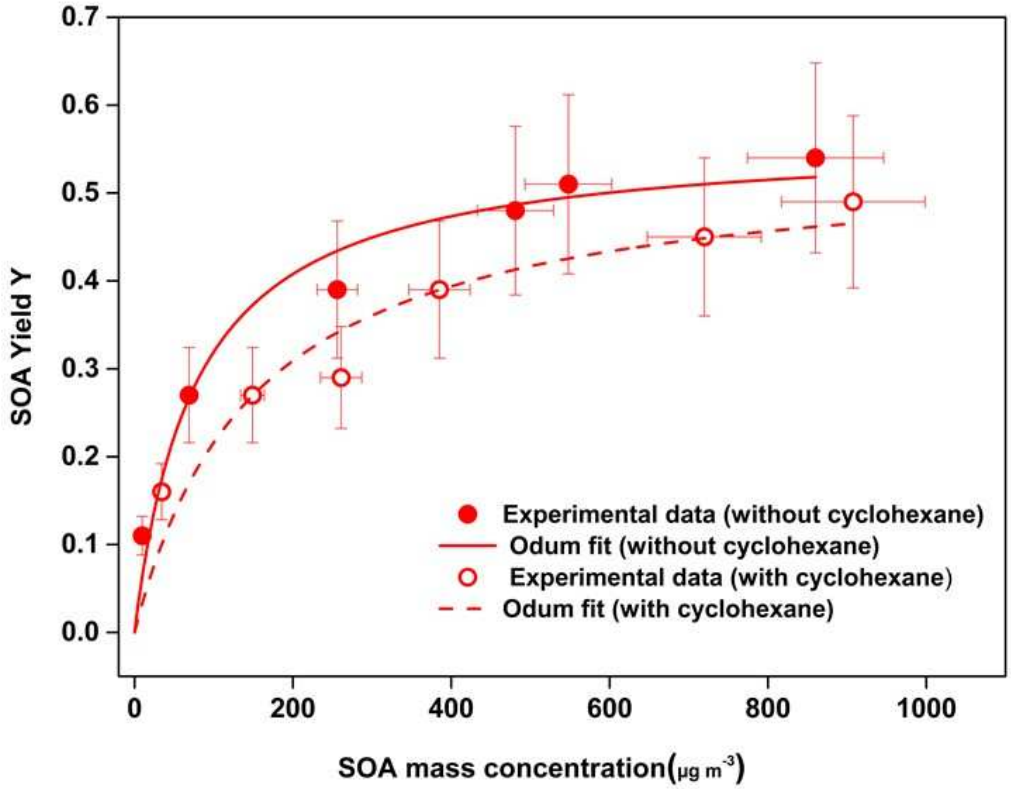

Fig. 5. Comparison of SOA yields formed from the γ-terpinene ozonolysis with those from other monoterpenes measured under similar experimental conditions in the presence of cyclohexane. The mass-dependent yield data reported in previous studies were recalculated using an aerosol density of (1.5 ± 3) g cm^{-3} for comparison (the error barres correspond to the SOA density range). Lines are the best empirical Odum model fits considering one semi-volatile major product.

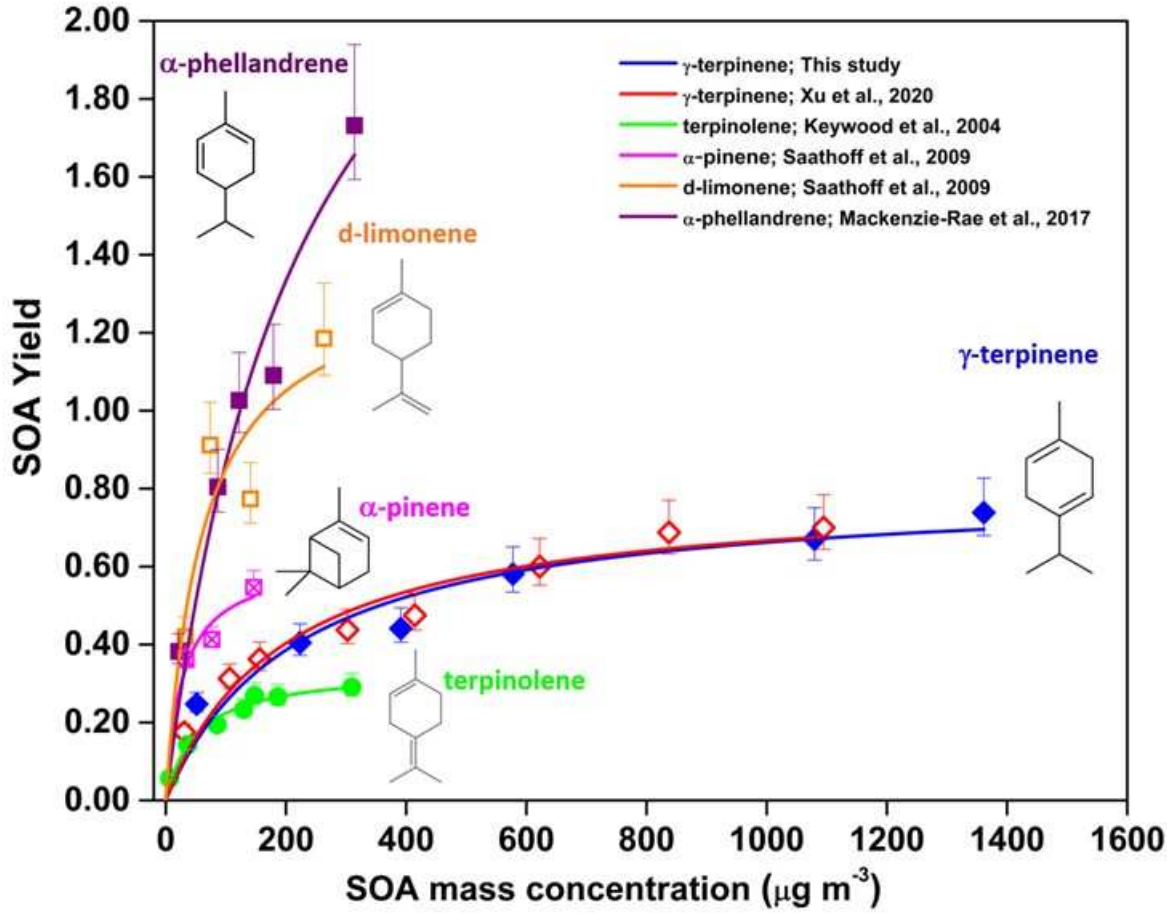

Fig. 6. SEM images of SOA particles. a) collected on lacey film (DP50 = 30 nm) at the end of exp. γ-terpinene#4 (left) and exp. γ-terpinene#10 (right); b) collected on carbon formvar film (DP50 = 30 nm) at the end of exp. γ-terpinene#4. Exp. γ-terpinene#4 and γ-terpinene#10 were performed, without and with an OH radical scavenger (cyclohexane), respectively.

a)

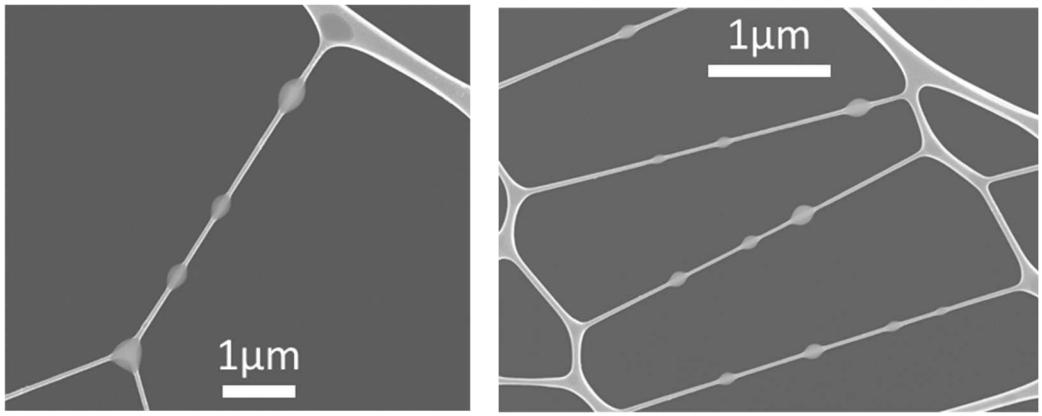

b)

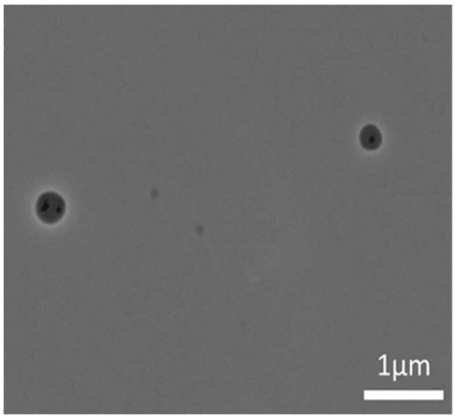

Table 1. Summary of experimental conditions and results for the SOA formation from the ozonolysis reaction of γ-terpinene.

	Exp.	$[\gamma\text{-terp}]_0$[a]		$[O_3]_0$[b]	$\Delta[\gamma\text{-terp}]$[c]	M_0[d]	Yield (Y)[e]
		(ppbv)	(μg m^{-3})	(ppbv)	(μg m^{-3})	(μg m^{-3})	
Without cyclohexane	γ-terpinene#1	16	90	60	86	10	0.11
	γ-terpinene#2	47	266	101	253	69	0.27
	γ-terpinene#3	117	664	424	654	256	0.39
	γ-terpinene#4	158	895	268	878	410	0.47
	γ-terpinene#5	180	1020	300	1003	481	0.48
	γ-terpinene#6	192	1089	430	1079	548	0.51
	γ-terpinene#7	283	1604	621	1594	860	0.54
With cyclohexane	γ-terpinene#9	38	214	91	208	34	0.16
	γ-terpinene#10	99	561	280	552	148	0.27
	γ-terpinene#11	158	895	420	887	260	0.29
	γ-terpinene#12	177	1003	445	994	385	0.39
	γ-terpinene#13	285	1618	600	1610	719	0.45
	γ-terpinene#14	328	1856	625	1843	907	0.49

[a] Initial γ-terpinene concentration.

[b] Initial ozone concentration.

[c] Reacted γ-terpinene concentration.

[d] Organic aerosol mass concentration (corrected for wall losses).

[e] Overall SOA yield (Y) calculated as the ratio of M_0 to the total reacted γ-terpinene concentration.